

Coherence between superconducting edge states in superconducting periodic arrays of artificial defects

C.C. Abilio¹, L. Amico^{2,4}, Rosario Fazio^{2,3}, and B. Pannetier¹

¹*CNRS-CRTBT, Laboratoire associé à l'Université Joseph Fourier,
25 Av. des Martyrs, 38042 Grenoble Cedex 9, France*

²*Dip. di Metodologie Fisiche e Chimiche (DMFCI), Università di Catania,
viale A. Doria, I95219 Catania, Italy*

³*Istituto Nazionale di Fisica della Materia (INFM), Unità di Catania*

⁴*Dpto de Fisica Teorica de la Materia Condensada,
Universidad Autonoma de Madrid, Madrid E-28049, Spain.*

The transition line of superconducting arrays of holes exhibits a rich field structure due to the interference of superconducting states nucleated at the holes edges. We studied by means of resistance measurements their effect on the $T_c^(H)$ line as a function of transverse magnetic field using regular arrays of nanofabricated micron size holes. The arrays transition fields are higher than for the bulk. Moreover we found a nontrivial field modulation of the $T_c^*(H)$ line with an inversion, with increasing field, of the modulation concavity which we assigned to a crossover from a collective to an isolated edge state regime. The high field regime is well described by the nucleation at a single hole in an infinite film. The modulation at low fields was found to be dominated by the interference of neighbor edge states when the inter-hole distance w becomes comparable to the coherence length $\xi(T_c^*)$. A comparison between arrays of different hole shape shows the influence of geometry on the type of interaction established, which can be described either as a superconducting wire network or as a weak link array.*

PACS numbers: 74.76, 74.60, 74.25

1. Introduction

The effect of artificial pinning centers on the vortex dynamics of type-II superconductors has attracted a great interest in both fields of high T_c and conventional low T_c superconductors. Low T_c materials are particularly interesting due to the development of nanofabrication techniques which enable the introduction in a controlled way of nanofabricated defects. These patterned samples constitute relatively simple systems for the study of how geometric parameters such as defect size, shape and/or defect density influence vortex dynamics^{1,2,3}.

Previous experiments on superconducting arrays of holes have shown that the transition line is dominated by surface superconducting states nucleated around the hole boundaries¹. As a result, the array transition occurs at fields H_{c3}^* higher than the nucleation fields in the bulk H_{c2} , and the transition line $T_c^*(H)$ exhibits a non-trivial field modulation due to flux quantization of the edge states over the two geometric lengths of the problem: the hole surface and the array elementary cell. In particular, it was identified a crossover with decreasing field from an isolated hole regime to a low field regime dominated by the interaction between edge states. Though the behavior at high fields was well understood, the nature of the interactions at low fields remained unclear.

In this paper we address in detail the collective regime at low fields when the distance between adjacent holes edges w is comparable to the array lattice constant a . The relevant parameters are the external field, the temperature dependent coherence length $\xi(T_c^*)$, the lattice constant a , the hole size, and the inter-hole distance w . We will try to put forward the role of these parameters on the crossover to the collective regime and the type of interaction established at low fields. The two extreme cases, the isolated hole in an infinite film⁴ and the superconducting wire network^{5,6} (vanishing hole separation) are quite well known.

In section 2. we present transport measurements on a superconducting square array where the aspect ratio hole size/lattice parameter is approximately two. These results are compared in section 3. with our previous work¹ on a different array with similar aspect hole/lattice parameter but with twice the distance between hole edges. The distinct behavior found at low fields will be discussed as arising from distinct nucleation processes, determined by the ratio w/ξ . In section 3.2. we analyze the case where $w/\xi(T_c^*)$ is lower than the critical ratio 1.84⁷. Nucleation is then dominated by thin wire superconducting edge states and the coupling between them is well described by the formalism of superconducting wire networks^{5,6}. In section 3.3. we analyze the case $w/\xi(T_c^*) > 1.84$ where edge nucleation is de-

terminated at the single hole edge but w is still small enough to allow a weak overlap between neighbor edge state wave functions. In this regime the low field behavior can be described using a model based on a weak link interaction between adjacent edge states. This simple model is able to capture the essential features of the crossover previously discovered ¹.

2. Experimental Details

The array sample consists of a thin film of aluminum (80 nm) patterned with a regular square array of nanofabricated holes. The lattice spacing is $4.0 \mu\text{m}$ and holes have a square shape with $1.85 \pm 0.01 \mu\text{m}$ side length, the distance between neighbor hole edges being $w = 2.15 \pm 0.01 \mu\text{m}$ as determined by SEM microscopy. We shall refer to this sample as sample A. The full array size is $1 \times 1 \text{ cm}^2$ corresponding to a total of 6.25×10^6 holes.

The patterning was defined on a monolayer PMMA coated 2" Si wafer by Deep UV photolithography using a high precision chromium mask⁸. The sample is then prepared using conventional *lift-off* techniques after thermal evaporation of pure aluminum over the resist mask on a UHV chamber. An homogeneous thin film of aluminum evaporated at the same time and submitted to the same fabrication steps is also measured for a reference of the patterning process effect on the material parameters.

Both samples were studied by conventional four-probe resistance measurements using an AC four terminal resistance bridge at a 33 Hz frequency and a measuring current of 2 nA. Assuming an uniform current distribution over the array, the current density per wire is $4.5 \times 10^{-4} \text{ A cm}^{-2}$. We used a similar in-line geometry for the voltage contacts (spiral-shaped) in the array sample as in our previous work ¹, placed at a distance of 2.8 mm from each other in the array center to avoid short circuits from the sample borders. For the reference sample we simply attached gold (non-superconducting) wires by ultrasonic bonding. No overshoot in the $R(T)$ curves was observed, in contrast to the previously studied reference sample ¹ where the spiral contacts were used and small cusps in the $R(T)$ curves were present. ¹

Resistance measurements as a function of temperature were also performed at several magnetic fields between 0 and 5 mT. From the zero field $R(T)$ measurement we estimated several material parameters. Using a two-

¹We remark that the $R(T)$ curves for array A in non zero field do not exhibit the double transition observed on array B, which was then assigned to a first transition at T_{c2} and to a second transition at higher temperatures T_c^* . We now believe the observation of the T_{c2} transition in array B was possible due to the transition of the $20 \mu\text{m}$ strips between patterned fields (of about $300 \times 300 \mu\text{m}^2$). In the case of array A, which is an homogeneous pattern over a 1 cm^2 surface, the double transition is not observed.

dimensional Aslamazov-Larkin fit ⁹, we estimate a BCS transition temperature $T_{co} = 1.262$ K and a normal state resistance of $R_n = 0.099$ Ω . The resistance per single wire of length $a = 4.0$ μm and width $w = 2.15$ μm is then $r_n = 0.354$ Ω and the normal state resistivity $\rho_n = 1.49$ $\mu\Omega\text{cm}$. Using $v_F = 2.03 \times 10^8$ cm/s we obtain an electronic mean free path $l_{el} = 26.5$ nm. The zero field transition temperature defined at half of the normal state resistance are 1.263 K and 1.265 K for the patterned sample and the homogeneous thin film, respectively, the transition width being 3 mK for both samples. We summarize on Table 1 some parameters of array A and the parameters of the sample previously studied ¹, array B. This array consists on an aluminum thin film (80 nm thickness) patterned with a square array of circular holes of diameter $2r = 4.26$ μm and a lattice parameter of 9.0 μm .

The field dependence of the nucleation temperatures $T_c^*(H)$ is determined using a heating feedback technique that keeps the sample resistance at a constant value while the magnetic induction field is smoothly varied by small increments of 0.2 μT . This method enables us to attain a fine field tuning of the array transition line. Several resistance criteria between 0.01 and $0.7R_n$ were used. The nucleation temperatures using the sweeping field method agree by less than 1 mK with those obtained for the same resistance criteria from $R(T)$ measurements, indicating a good temperature regulation attained by the feedback method.

The transition line $T_c^*(H)$ of array A for criteria $0.4R_n$ is displayed in Fig. 1.a) as a function of applied field. For comparison it is also displayed the reconstructed bulk transition line, $H_{c2}(T^*/T_{co}) = (1 - T^*/T_{co}) \Phi_0/2\pi\xi^2(0)$, using the reference film coherence length at $T = 0$ K, $\xi(0) = 220$ nm (determined from the initial linear slope of the reference film transition line). The array transition line is clearly above the estimation for the bulk. Besides, the non-trivial field modulation associated to the single hole and collective regimes are clearly identified. At fields below 0.75 mT it is characterized by periodic upward cusps, with a magnetic period of exactly $H = 0.128$ mT, that correspond to a quantum flux enclosed on a square cell of side length $a = 4.0$ μm , indicating the presence of phase coherence over the array lattice. At higher fields, the transition line exhibits downward dips occurring with a larger magnetic period. These large period oscillations correspond to the single hole regime discussed previously. In this case, the magnetic period is not constant since it depends on the effective surface formed by the hole radius and the surface superconducting sheath surrounding the hole. The average magnetic period is 0.543 mT, which corresponds to an effective square surface of side length $l_{hole} = 1.94$ μm , comparable to the array hole size of 1.85 μm .

These field modulations were found for all the criteria used in the tran-

sition line measurement. The crossover between the two field regimes is well illustrated on Fig. 1.b) where the sawtooth variation of the transition line slope $dT_c^*(H)/dH$, at low field gives place to a smoother variation at higher fields, along with the change of magnetic period.

3. Discussion

3.1. Extraction of the energies for nucleation of superconductivity

The role of the nucleation processes involved will be discussed in terms of the energies for nucleation of superconductivity at a given field, ϵ_{nucl} . The energy ϵ_{nucl} can be obtained by finding the lowest eigenvalue solution of the linear Ginzburg Landau differential equation

$$\frac{\hbar^2}{4m} \left[\frac{\nabla}{i} - \frac{2e}{c} \mathbf{A} \right]^2 \psi(\mathbf{r}) = \epsilon_{nucl} \psi(\mathbf{r}) \quad (1)$$

which fulfills the given boundary conditions on the order parameter $\psi(\mathbf{r})$.

This approach is valid when we can neglect spatial variations of $|\psi(\mathbf{r})|$, such as thin films or wires of thickness $\ll \xi$ or when the applied magnetic field reduces $|\psi(\mathbf{r})|$ to a value much smaller than the equilibrium amplitude $|\psi_\infty|$ achieved deep inside the bulk superconductor. The regime of validity is then usually restricted to temperatures close to T_{co} .

An alternate approach is to extract ϵ_{nucl} at a given field from the measured $T_c^*(H)$ using the relation ^{10,11},

$$\ln \left[\frac{T_c^*}{T_{co}} \right] = \Psi_D \left[\frac{1}{2} \right] - \Psi_D \left[\frac{1}{2} + \frac{\epsilon_{nucl}}{4\pi k_B T_c^*} \right] \quad (2)$$

where $\Psi_D(x) = \Gamma'(x)/\Gamma(x)$ is the digamma function. This relation describes the depression of $T_c^*(H)$ relative to T_{co} due to a magnetic perturbation. Though it was initially established by Abrikosov and Gor'kov for magnetic impurities ¹⁰, it can be generalized to all pair breaking perturbations which destroy the time reversal symmetry of Cooper pairs ^{11,12}, if the scattering time of the electron pair is short enough for their relative phases be randomized by the perturbation.

It can thus be applied to a dirty superconductor in strong external magnetic fields (and only surrounded by insulators), if the mean free path l_{el} is much smaller than all sample dimensions and ξ_o or in the case of a small superconducting particle with all dimensions $\ll \xi_o$. The sample thickness must be smaller than ξ and the penetration depth to ensure the penetration

of the magnetic field. At temperatures close to $T_c^*(H)$, ϵ_{nucl} is the energy required to break the Cooper pair thus destroying superconductivity. When $T_c^* = 0$, (or $H = H_{c3}^*(0)$), ϵ_{nucl} coincides with the BCS superconducting gap $1.76k_B T_{co}$. Close to T_{co} the digamma function can be expanded around 1/2 and the $T_c^*(H)$ depression is linear in ϵ_{nucl} , $T_{co} - T_c^*(H) = \epsilon_{nucl}\pi/8k_B$.

The advantage of using Eq. 2 on the determination of ϵ_{nucl} is that it remains valid down to all temperatures and in strong magnetic fields. The linear Ginzburg-Landau results can be recovered if the temperature dependent coherence length is defined as $\xi^2(T) = D\hbar/\epsilon_{nucl}$, where $D = 1/3v_F l_{el}$ is the coefficient for electronic diffusion. For sample A, $D = 180 \text{ cm}^2\text{s}^{-1}$ obtained from the mean free path $l_{el} = 26.5 \text{ nm}$. Using $\xi^2(0) = \hbar D / (1.76k_B T_{co})$ we estimate $\xi(0) = 250 \text{ nm}$.

We calculated $\epsilon_{nucl}(H)$ for arrays A and B using Eq. 2 and the experimental T_c^* at the given applied field H . These results are displayed in Fig. 2 after being normalized by the nucleation energy on the bulk, $\epsilon_{c2} = hDH/\Phi_o$, with the same coherence length as the array. For comparison, we also represent the theoretical $\epsilon_{nucl}/\epsilon_{c2}$ for a circular hole on an infinite film (solid line) ¹³. In fact, the representation $\epsilon_{nucl}/\epsilon_{c2}$ is equivalent to the inverse ratio of the nucleation fields H_{c2}/H_{c3}^* , that close to T_{co} acquires the Ginzburg Landau form $H_{c2}/H_{c3}^* = (1 - T_c^*/T_{co}) H_{c2}(0)/H$, using $H_{c2}(0) = \Phi_o/2\pi\xi^2(0)$ and the coherence length as defined above.

From Fig. 2 it is clear that in the high field regime both samples are very well described by the theoretical single hole case. With decreasing fields both arrays deviate from the single hole description, with the appearance of the collective field modulation, periodic on Φ_o per array cell, and with upward concavity. It is in this regime that the samples present a strikingly distinct behavior. The reduced energies $\epsilon_{nucl}/\epsilon_{c2}$ for sample B and for the single hole tend to an overall increase with decreasing field, reaching 1 at zero field. In contrast, for sample A, $\epsilon_{nucl}/\epsilon_{c2}$ decrease with decreasing field, dropping well below the single hole line. This means that in this regime, array A presents a ratio H_{c3}^*/H_{c2} higher than the classical limit of 1.69 for an infinite surface sheath⁷. Comparing the array geometric parameters, they both have similar aspect ratios w/a , 0.54 (array A) and 0.53 (array B), respectively and similar ratios of the superconducting volume over the array cell volume V_s/V_{cell} , 0.79 (array A) and 0.82 (array B). We thus believe the distinct low field behavior is associated to the different ratio $w/\xi(T_c^*)$, which close to T_{co} controls the process of edge nucleation and the type of coupling. In fact, both samples loose the collective behavior for $w/\xi(T_c^*) > 3$.

On the following subsections we shall analyze these features by describing the array nucleation energy as coming from two main contributions: the nucleation energy of the single edge state and the coupling energy between

neighbor edge states.

3.2. Wire networks of wide strands

In this section we focus on the low field behavior of array A. In this regime, the array energy is a sum of the nucleation energy on a individual wire in parallel field $\epsilon_{strip\parallel}$ and a coupling energy, that can be described within the framework of superconducting wire networks theory ^{5,6}.

The case of superconducting wire networks of narrow wires is well understood. It can be treated as a periodic array of superconducting islands strongly coupled to each other by thin superconducting wires of length a ($\xi \gg a$) and width $w \ll \xi$. Neglecting superconducting fluctuations, the coupling energy can be computed within mean-field theory by solving the linearized Ginzburg-Landau equations at each node of the network. For a regular square lattice (same length of all strands) the order parameter ψ_i on each island i will be coupled to the first neighbor sites through field dependent phase factors as,

$$4 \cos(u) \psi_i = \sum_j \psi_j \exp(-i\gamma_{ij}) \quad (3)$$

where 4 is the lattice coordination, $\gamma_{ij} = 2\pi/\Phi_0 \int_i^j \mathbf{A} \cdot d\mathbf{l}$ is the phase factor along the wire linking site i to a site j , \mathbf{A} the vector potential, and $u = a/\xi(T)$ is the strand length in units of $\xi(T)$. The coupling energy is then given by, $\epsilon_{wnt} = \hbar Du^2/a^2$.

Eq. 3 is equivalent to a tight binding equation in a potential with the same geometry and tight binding energy $\epsilon_{tb} = 4 \cos u$. The network coupling energy $\epsilon_{wnt} = \hbar Du^2/a^2$ can then be expressed in terms of the tight binding ground state level ϵ_{tb} with $u = \arccos(\epsilon_{tb}/4)$ ^{14,15}. However, this relation is only valid in the limit $w \gg \xi$. Taking into account the finite thickness of the wires, a more complex relation between ϵ_{tb} and u is obtained, $\epsilon_{tb} = 4 \cos u + 4 \tan(uw/2a) \sin u - uw/a$ ¹⁶. This result was established for zero external field but it can still be applied at low fields while there are no vortices in the wires.

In the inset of Fig. 3 is displayed the coupling energy of array A and the theoretical ϵ_{wnt} energy as a function of magnetic flux per array elementary cell Φ_{cell} , for Φ_{cell}/Φ_0 between 0 and 1. The coupling energy for array A is obtained from ϵ_{nucl} (calculated using Eq. 2 and the experimental $T_c^*(H)$) after subtracting the parabolic energy contribution due to edge nucleation in the wires, $\epsilon_{strip\parallel}$. The theoretical ϵ_{wnt} is obtained from the ground state tight binding energy calculated for rational values of $\Phi_{cell}/\Phi_0 = p/q$, with

$q < 30$ and $p < q$. A very good agreement is obtained between the experimental and the theoretical data which take into account the wire thickness. The theoretical results in the limit $w = 0$ lead to a smaller energy. Since we are close to T_{co} , the variation of $T_{co} - T_c^*(H)$ due to the coupling (after subtracting the linear dependence on H) corresponds to $\epsilon_{wnt}\pi/8k_B$.

Besides the fundamental dips at $\Phi_{cell}/\Phi_o = 0, 1$ and at $1/2$, additional dips can be identified at rational values $\Phi_{cell}/\Phi_o = p/q$, for $q = 3, 4$ and 5 . This field structure is a manifestation of the interference of quantum states over cells of size $qa \times qa$ ¹⁵. With increasing field, the fine field structure becomes less pronounced and only the fundamental dips remain until $\Phi_{cell}/\Phi_o = 8$. At higher fields the single hole regime is recovered.

In fact, the crossover to the single hole regime is associated to a crossover from a two-boundary to a one-boundary nucleation process in the network wires. This explains the smaller values of $\epsilon_{nucl}/\epsilon_{c2}$ when compared to the classical limit $\epsilon_{nucl}/\epsilon_{c2} = 0.59$ for nucleation in an infinite surface sheath⁷ or for nucleation in a single hole. Such as for a thin slab in a parallel field, edge nucleation in the array at low fields is controlled by two boundary conditions imposed at the edges of adjacent holes.

The field dependence of $\epsilon_{strip \parallel}$ for a strip or slab of intermediate thickness w , is strongly dependent on $w/\xi(T_c^*)$. Below a critical thickness $w < 1.84 \xi(T_c^*)$ (thin wire limit) nucleation starts symmetrically at both surfaces and the maximum of the order parameter occurs at middle distance between them. In this limit $\epsilon_{strip \parallel} = H^2 w^2 (\pi h D / 6 \Phi_o^2)$. With increasing field, when $w > 1.84 \xi(T_c^*)$, $\epsilon_{strip \parallel}$ deviates from the parabolic field dependence as the order parameter solutions at each surface pull apart, their superposition giving rise to nodes along the middle plane of the wire and equidistant of $\Delta L \approx \Phi_o / H w (1 - 1.84 \xi)$. With increasing field the vortex pattern becomes more complex, until the interference between the surface solutions become negligible (compared to $k_B T_c^*$) and the one-boundary solution is recovered. In this limit $\epsilon_{strip \parallel}$ approaches the surface sheath result $0.59 h D H / \Phi_o$.

All these features were discussed previously^{7,17,18}. Here we are interested in comparing the envelope of the energy curve for array A and the nucleation energy for a strip, $\epsilon_{strip \parallel}$. On Fig. 3 is displayed ϵ_{nucl} for array A and $\epsilon_{strip \parallel}$ for a wire with the same width w as the array strands as a function of applied field. We can identify several similitudes. On the single hole regime the main dependence of ϵ_{nucl} is linear on H such as the field dependence of $\epsilon_{strip \parallel}$ in the surface sheath limit, in agreement with the dominance of one-boundary nucleation at the edges of each individual hole. With decreasing field both curves deviate from the linear field dependence due to the emergence of interference between adjacent surfaces solutions. This deviation occurs near the field $H_1 = 0.65$ mT which corresponds to the

position of the first important collective dip of $\epsilon_{nucl}/\epsilon_{c2}$ at $\Phi_{cell}/\Phi_o = 5$ (see also Fig. 4.b). Below the field $H_o \approx 2.75 \Phi_o/\pi w^2$ (0.39 mT) nucleation starts symmetrically⁷ in the strip and the order parameter is maximum at middle distance between adjacent edges. The occurrence of symmetric nucleation on a low field regime explains why the wire network description is still valid for arrays of wide strands. In the regime $H < H_o$, the collective dips of ϵ_{nucl} approach the parabolic envelope $\epsilon_{strip} \parallel$, since at integers values of Φ_{cell}/Φ_o the costs in coupling energy are minimum. These results thus indicate that the small values of $\epsilon_{nucl}/\epsilon_{c2}$ for array A at low fields are simply related with the two-boundary nucleation process.

On the other hand, since the crossover from two-boundary to one-boundary nucleation is associated to the appearance of interstitial nodes of the order parameter within strands, we expect a broadening of the array resistive transition with increasing field due to these weakly bounded interstitial vortices. In Fig. 4 is represented the field variation of the resistive transition width $\Delta T_c^*(H)$, for array A obtained by subtracting the transition lines $T_c^*(H)$ measured for resistive criteria $0.7R_n$ and $0.03R_n$. For comparison, we also represent the field variation of the distance ΔL between nodes on a single wire, normalized by the array lattice parameter $a = 4 \mu\text{m}$.

At fields $H \leq H_o = 0.39 \text{ mT}$ (region I, $\Phi_{cell}/\Phi_o \leq 3$) the transition width at integers Φ_{cell}/Φ_o is the same as in zero field since there are no order parameter nodes in the strands, only coreless vortices inside holes. At integers Φ_{cell}/Φ_o , the flux quanta per array cell corresponds to the quanta enclosed by each hole. The transition is then sharpened since every hole encloses the same number of flux quanta. At intermediate values of Φ_{cell}/Φ_o phase fluctuations lead to a small broadening of the transition (of about 1 mK).

At fields $H_o < H < H_1$ (region II, $3 < \Phi_{cell}/\Phi_o < 5$), the first nodes of the order parameter are expected to appear within the strands with a separation ΔL that drops from infinity to values comparable to the array lattice parameter. In this regime there will be a competition between increasing the flux per hole by Φ_o or follow the increase of field by accommodating vortices at interstitial positions in the array wires. The increase of the transition width for Φ_{cell}/Φ_o between 4 and 5 illustrates the presence of a few loosely bound vortices. This observation is in agreement with Fig. 4.b) where the field dependence of $\epsilon_{nucl}/\epsilon_{c2}$ represented as a function of Φ_{cell}/Φ_o shows that $\epsilon_{nucl}/\epsilon_{c2}$ at $\Phi_{cell}/\Phi_o = 4$ is higher than the adjacent dips. At $\Phi_{cell}/\Phi_o = 5$ every hole encloses 4 Φ_o which favors the decrease of $\epsilon_{nucl}/\epsilon_{c2}$. Also, the distance between vortices in the strands should be of the order of a and, in that case, they can occupy positions at the array interstices forming a stable sub-lattice, which decreases the resistive transition width.

In region III, the distance between interstitial vortices should drop below a and the transition width broadens considerably due to these weakly bounded vortices. The distance between nodes is further reduced with increasing field until edge states at each hole become independent.

We can see from Fig. 4.b) that at $\Phi_{cell} = 8 \Phi_o$, the field modulation of $\epsilon_{nucl}/\epsilon_{c2}$ inverts concavity once the single hole nucleation becomes dominant. If for Φ_{cell}/Φ_o between 5 and 8, the additional flux occupies interstitial positions, the flux per hole remaining equal to $4 \Phi_o$, $\epsilon_{nucl}/\epsilon_{c2}$ should meet the single hole curve at its 4th oscillation, in agreement with the results presented on Fig. 2.

3.3. Weak link array of edge states

We do not expect the description of a wire network of wide strands to hold if holes edges are pulled apart and/or shaped to circles. This is the case of sample B where the minimum inter-hole distance is $w = 4.74 \mu\text{m}$ (\sim twice compared to array A). The field for symmetric nucleation is $H_o \approx 0.08 \text{ mT}$ for a stripe with the same thickness. However since the distance between hole edges is not constant (varying from 4.74 to $9 \mu\text{m}$ around the hole perimeter) H_o should be further reduced. As a consequence the parabolic envelope of ϵ_{nucl} is not observed. The coupling between neighbor edge states is still present though. Fundamental dips of ϵ_{nucl} at integers values of $\Phi_{cell}/\Phi_o \leq 7$ are clearly observed although we find no fine field structure ¹⁹. At low field $\epsilon_{nucl}/\epsilon_{c2}$ is lower than the single hole calculation indicating that the energy contribution due to the overlap between edge states is important.

In the next sections we present a simple model which is able to capture the transition from the single hole to the collective behavior for array B. The application of this model is based on the assumption that in a narrow temperature region $T_{c2} < T < T_c^*$ the superconducting edge states are localized close to the hole boundaries and the system behaves like an array of weak links. The fast oscillations observed at low fields are then related to the collective behavior of the array. Since there is nonzero overlap between the wave functions of different edges, the energy should be higher than that of a single hole. One consequence is that the nucleation field H_{c3}^* is lower than that of a single hole, as it is observed in the experiments. The single hole behavior is naturally recovered at higher fields where the overlap between neighboring edges vanishes.

A Ginzburg-Landau approach is suitable to study the problem. For the single hole, an analytical solution is available due to the cylindric symmetry of the problem ²⁰. A variational approach for the determination of the order

parameter has been analyzed by Buzdin ⁴. The agreement with the exact solution is good except at low fields where the variational approach predicts a region with zero flux through the hole which is not present in the exact solution. Buzdin's variational approach, however, has the great advantage of being applicable also in the many holes case where an analytical solution is impossible to obtain.

We proceed as follows. We first describe an improved variational ansatz for the single hole case by using a trial order parameter of three parameters. We then construct an effective Ginzburg-Landau free energy which takes into account, in an approximate way, the edge coupling and we determine the resulting nucleation energy.

3.4. Variational approach : single hole

In this section we introduce the new variational wave function for the evaluation of the nucleation energy in a superconducting film containing a hole. Following Buzdin ⁴, the Ginzburg-Landau free energy (\mathcal{F}_N is the free energy of the normal state) is given by

$$\mathcal{F} - \mathcal{F}_N = \frac{\hbar^2}{4m} \int d^2r \left[\left| \left(-i\nabla - \frac{2\pi}{\Phi_o} \mathbf{A} \right) \psi(\vec{r}) \right|^2 - \frac{1}{\xi^2} |\psi(\vec{r})|^2 \right] \quad (4)$$

The fourth order term has been ignored since we are interested in the phase boundary. The surface critical field can be determined with a variational procedure by determining the minimum of the functional

$$\mathcal{F} - \mathcal{F}_N = 0 \quad (5)$$

within the class of trial wave functions $\psi(\vec{r})$ which satisfy the proper boundary condition at the superconductor-insulator interface

$$\left[\frac{\partial \psi}{\partial \rho} \right]_{\rho=R} = 0 \quad (6)$$

where R is the radius of the hole. For a hole containing m flux quantum, the order parameter has the following form in cylindric coordinates (ρ, ϕ, z) ,

$$\psi = \frac{1}{\sqrt{2\pi}} F(\rho) e^{im\phi}$$

. It is possible to improve the result obtained by ²¹ by using a three-parameters trial order parameter of the form

$$F(x) = \left[1 + \alpha(x - x_0)^\eta + \beta(x - x_0)^\zeta \right] \exp \left[-\frac{\gamma}{2}(x - x_0)^2 \right] \quad (7)$$

where α, β, γ are the variational parameters and the dimensionless quantities $x = \rho(eH/c\hbar)^{1/2}$, $x_0 = R(eH/c\hbar)^{1/2} = (\Phi_{hole}/\Phi_o)^{1/2}$ has been introduced.

For the case of a single hole an exact solution for the nucleation energy is expressed in terms of the eigenvalues of the Kummer's equation ^{20,22}. We compare our results (the best results have been obtained for $\eta = 2$ and $\zeta = 2.05$) with the exact calculation and with the one parameter trial function ⁴. This is shown in Fig. 5. The trial function $F(x)$ given by Eq. (7) has a maximum at $(x - x_0)^2 \sim (2 - \gamma/(\alpha + \beta))/\gamma$, a feature which is also present in the exact solution. This seems to improve considerably the accuracy of the variational approach ²³.

The result obtained by using Eq. (7) improves considerably the agreement with the exact solution. In particular the spurious $m = 0$ is shrunk to very low fields ($< 0.03 \Phi_o$).

3.5. Variational approach : array of holes

We obtain an approximate expression of the nucleation energy for a regular array using the variational wave function introduced in the previous section and an appropriate Ginzburg-Landau free energy which takes into account the overlap between edge states of adjacent holes. The model is sketched in Fig. 6, we will consider an array of edges connected by weak links (dashed lines in the figure). The crossover between the single hole and the collective behavior stems from the interplay of flux quantization on each hole and frustration effects through the elementary array cell.

The GL free energy which we propose has the following form

$$\mathcal{F} - \mathcal{F}_N = \sum_i \mathcal{F}_i + \sum_{\langle i,j \rangle} \mathcal{F}_{ij} \quad (8)$$

where \mathcal{F}_i is the free energy defined in Eq. (4) and the subscript i identifies the hole in the array. \mathcal{F}_{ij} takes into account the overlap between the holes.

We choose a \mathcal{F}_{ij} of the following form

$$\mathcal{F}_{ij} = \frac{\hbar^2}{4ma^2} \int d^2r \left[\alpha_o |\psi_i(\vec{r}) - \psi_j(\vec{r})|^2 + (\alpha_1 + \alpha_2 \delta_{ij}) |\psi_i(\vec{r})| |\psi_j(\vec{r})| \right] \quad (9)$$

The effect of the external magnetic field will be included in Eq. 9 by means of a Peierls substitution. We assume that the overlap is restricted to a small area (see the dashed lines in Fig. 6) and that the hole array can be treated as a weak link array. The first term in Eq. 9 is modified as follows

$$|\psi_i - \psi_j|^2 \rightarrow |\psi_i|^2 + |\psi_j|^2 - 2|\psi_i||\psi_j| \cos(\phi_i - \phi_j - \pi m - A_{ij}) \quad (10)$$

where $A_{i,j} = (2\pi)/(\Phi_o) \int_i^j \mathbf{A} \cdot d\mathbf{l}$ is calculated along the path indicated by the dashed lines in Fig. 6 (we assumed that all the holes contain the same number m of flux quantum).

The terms in Eq. 9 can be understood considering that the order parameter in the array of holes can be given as $\psi = \sum_i \psi_i$. Substituting this expression in the GL free energy of Eq. 4, one generates the various terms given above. In general since the approach is phenomenological, the various contributions enter with different coefficients ($\alpha_o, \alpha_1, \alpha_2$). It is important to stress that the total wave function does *not* satisfy the proper boundary conditions around the holes because of the exponential tails of the edge states of the neighboring island. Therefore this approach breaks down at very small field when the overlap becomes too strong.

The agreement of the experiments with the single hole result in the high flux regime indicates that phase fluctuations do not drive the phase transition. In this case we can approximate the phase dependent part of the free energy by its ground state energy

$$\epsilon(\Phi_{cell}/\Phi_o) = \frac{2}{zN} \sum_{\langle i,j \rangle} \langle \cos(\phi_i - \phi_j - \pi m - A_{ij}) \rangle_{GS}$$

where N is the number of holes in the array, z is the coordination number, Φ_{cell}/Φ_o is the magnetic flux per elementary cell of the array and $\langle \dots \rangle_{GS}$ means the ground state configuration of the phases ϕ_i .

Going over the same steps as Buzdin ⁴ the nucleation energy for an array of holes is obtained by minimizing the following functional over the trial function introduced in Eq. 7

$$\begin{aligned} \frac{\epsilon_{nucl}}{\epsilon_{c2}} &= \mathcal{I} \int_{x_0}^{\infty} \frac{dx}{x} \left[(m - x^2)^2 F^2(x) + x^2 [F'(x)]^2 + g \frac{R^2}{a^2} \frac{1}{4x_0^2} x^2 [F(x)]^2 \right] \\ &+ g_1 \frac{R^2}{a^2} \frac{1}{4x_0^2} [2 - g_2 \epsilon(\Phi_{cell}/\Phi_o)] \langle F(x_i) F(x_j) \rangle \end{aligned} \quad (11)$$

where the overlap integral

$$\langle F(x_i) F(x_j) \rangle = \mathcal{I} \int d\vec{x} F(\vec{x}) F(\vec{x} + \frac{\vec{w}}{x_0}) \quad (12)$$

the normalization

$$\mathcal{I}^{-1} = 2 \int_{x_0}^{\infty} dx x F^2(x)$$

has been introduced. The new parameters g, g_1, g_2 are easily expressed as a function of the α 's.

In Fig. 7 we present the results obtained for various values of the three parameters g, g_1 and g_2 . We can observe that the presence of the Josephson coupling increases the array nucleation energy, relatively to the isolated hole case, and introduces cusps of different concavity superimposed over the main single hole background at low flux when the coupling becomes stronger. These features were found in the experiment of Bezryadin *et al* ¹. At very low fields $\epsilon_{nucl}/\epsilon_{c2}$ rapidly increases, as also seen in the experiments. It may be explained by the fact the the wave functions extends over various lattice constants and therefore the system does not show any surface superconductivity. However this model breaks down at flux typically of the order of $0.15 \Phi_{hole}$.

A word of caution is needed at this point. Although the main features of the crossover are found one should be aware that the model is still too simplified to aim at a quantitative comparison with the experiments. In particular the choice of the values of the constants g is not related to any microscopic model which allow to justify the numerical parameters. It is, however, rewarding that most of the qualitative features are captured by our model. A further step might be to apply the techniques developed by Palacios *et al* ²⁴ to the present problem.

4. Conclusion

In conclusion, we tried to show how geometric parameters such as the inter-hole and the array lattice constant can influence the transition temperature of periodic superconducting arrays in a magnetic field.

We found a clear crossover with decreasing field from a single to a coupled edge state regime for both samples. The behavior of $\epsilon_{nucl}/\epsilon_{c2}$ in the single edge regime is very similar and the arrays transition depend exclusively on the magnetic flux per hole area. However, we remark that a quantitative comparison of the energy ratios $\epsilon_{nucl}/\epsilon_{c2}$ between samples need some caution since they are extremely dependent on the estimation of $\xi(0)$ and small errors can lead to a shift of the $\epsilon_{nucl}/\epsilon_{c2}$ values.

The low field behavior of the studied samples is representative of two distinct coupled systems: the superconducting wire network (strong coupling) and the weak link array. In both cases the coupling is mediated by the frustration induced by the applied field over the array elementary cell, however the type of coupling depends on the inter-hole distance w , the defect shape and the coherence length at $T_c^*(H)$ which controls the edge nucleation process. In the case of the weak link array (array B) we have a coupling of single hole edge states which depend on H through the enclosed flux per hole.

However, in the low field regime, the enclosed flux does not necessarily follow the field increase since the change of the hole winding number may be less favorable than placing flux at the array interstices where superconductivity is weakened. In the wire network case (array A at low fields), we have a strong coupling of the order parameter at the array nodes, which is non-zero along the wires due to symmetric nucleation. The flux enclosed per hole or per array cell are equivalent quantities as long as interstitial vortices are not allowed within the array strands. In this regime, the main contribution to the array transition comes from nucleation in the wires (which depends only on H).

This explains why the studied samples who have similar geometric ratios ($w/a \approx 2$ and $V_s/V_{cell} \approx 0.8$) exhibit such a different collective behavior. The relevant parameters are then the inter-hole distance (which allows two-boundary nucleation in a wide field regime for sample A) and the parallel hole edges which favor the thin wire nucleation. For periodic arrays of close enough ($w/\xi(T_c^*) < 1.84$) and parallel hole edges, the coupling between edge states can be described as a wire network coupling and the array transition approaches the thin wire nucleation at low fields. As a consequence, the ratio H_{c3}/H_{c2} ($\epsilon_{nuc}/\epsilon_{c2}$) in these arrays is not necessarily upper (lower) bounded by the surface sheath result $H_{c3}/H_{c2} = 1.69$ ($\epsilon_{nuc}/\epsilon_{c2} = 0.59$) or the single hole nucleation limit.

When two-boundary nucleation does not occur, due to a higher inter-hole distance and/or due to the hole shape, the wire network formalism is not suitable to describe the coupling between edge states, since the variations of the order parameter amplitude between holes cannot be neglected. In this case the array transition is dominated by single hole nucleation and we presented a coupling description, based in a weak link interaction between single edge states, which is able to recover the main features of the $T_c^*(H)$ line on the low field regime: the inversion of field modulation concavity and the presence of periodic upward cusps. In addition, it reproduces the experimental observation that the array transition occurs at temperatures below the single hole nucleation, since the array energy is increased due to the overlap between neighbor edge wave functions.

5. Acknowledgments

We would like to thank G. Falci and O. Buisson for useful discussions. We acknowledge the financial support of the European Community (Contract FMRX-CT-97-0143). C.C. Abilio is supported by a grant PRAXIS XXI (5713/95) of the Portuguese Ministry for Science and Technology.

REFERENCES

1. A. Bezryadin and B. Pannetier, *J. Low Temp. Phys.* **98**, 251 (1995). A. Bezryadin, and B. Pannetier, *Physica Scripta* **T66**, 225 (1996).
2. A.T. Fiory, A.F. Hebard, and S. Somekh, *Appl. Phys. Lett.* **32**, 73 (1978).
3. M. Baert, V.V. Metlushko, R. Jonckheere, V.V. Moschalkov, and Y. Bruynseraede, *Phys. Rev. Lett.* **74**, 3269 (1995).
4. A.I. Buzdin, *Phys. Rev B* **47**, 11416 (1993).
5. S. Alexander, *Phys. Rev. B* **27**, 1541 (1983).
6. R. Rammal, T.C. Lubensky, and G. Toulouse, *Phys. Rev. B* **27**, 2820 (1983).
7. D. Saint-James, and P.G. Gennes, *Phys. Lett.* **7**, 306 (1963).
8. 2 1/2 quartz plate fabricated by CSEM Neuchtel, Switzerland.
9. L.G. Aslamazov and A.I. Larkin, *Phys. Lett.* **26A**, 238 (1968).
10. A.A. Abrikosov, *Fundamentals of the theory of metals*, North-Holland (1988), Chap. 21.
11. P.G. de Gennes, *Superconductivity in Metals in Alloys*, (Benjamin, New York), 1966, Chap. 8.
12. K. Maki, *Superconductivity*, ed. R.D. Parks (Dekker, New York), 1969, ch.18.
13. A. Bezryadin, Yu.N. Ovchinkov and B. Pannetier, *Phys. Rev. B* **53**, 8553 (1996).
14. D.F. Hofstadter, *Phys. Rev. B* **14**, 2239 (1976).
15. B. Pannetier, J. Chaussy, R. Rammal and J.C. Villegier, *Phys. Rev. Lett.* **53**, 1845 (1984).
16. Y.Y. Wang, B. Doucot, R. Rammal and B. Pannetier, *Phys. Lett. A* **199**, 145 (1986).
17. H.J. Fink, *Phys. Rev.* **177**, 1017 (1969).
18. H.A. Schultens, *Z. Physik* **232**, 430 (1970).
19. The absence of fine field structure could be interpreted has due to the presence of coherence only at a first neighbors level or due to the amplitude oscillations being smaller than our temperature resolution.
20. A. Bezryadin, A.I. Buzdin, and B. Pannetier, *Phys. Rev. B* **51**, 3718 (1995); Yu.N. Ovchinnikov, *Sov. Phys. JETP* **52**, 755 (1980).
21. In Ref.4 Buzdin has chosen a trial form of $F(\rho)$ of the type $F(x) = \exp[-\frac{\gamma}{2}(x - x_0)^2]$.
22. R. Benoist and W. Zwerger, *Z. Phys. B* **103**, 377 (1997).
23. M. Tinkham, *Introduction to Superconductivity*, (Mac Graw-Hill New York, 1996).
24. J.J. Palacios, *Phys. Rev. B* **57**, 10873 (1998).

<i>Sample</i>	<i>hole shape</i>	<i>a</i> (μm)	<i>w</i> (μm)	<i>T_{co}</i> [K]	$\xi(0)$ (μm)
array A	square	4.0	2.15	1.263	0.25
	circle	9.0	4.74	1.25	0.25

Table 1. Some parameters of array A and array B. The array lattice constant is *a* and *w* the minimum distance between the edges of adjacent holes.

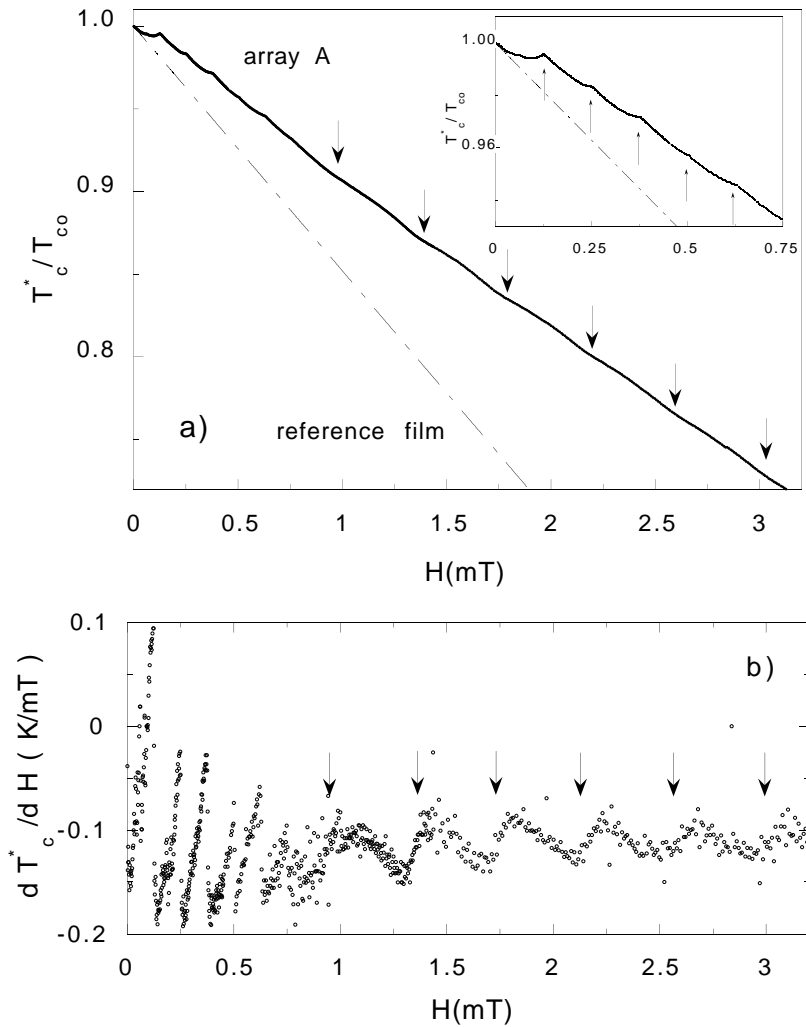


Fig. 1. a) Field dependence of the superconducting transition line $T_c^*(H)$ of array A (solid line) and of the reference sample $T_{c2}(H)$ (dashed line). Two types of field modulation are clearly identified for array A: downward, large period oscillations with dips at half integers of Φ_0 per hole (down arrows) and upward oscillations of shorter period with cusps at integers of Φ_0 per array elementary cell (inset:up arrows); b) $T_c^*(H)$ slope for array A as a function of H . The change of magnetic period due to the crossover from collective to single hole regime is quite visible.

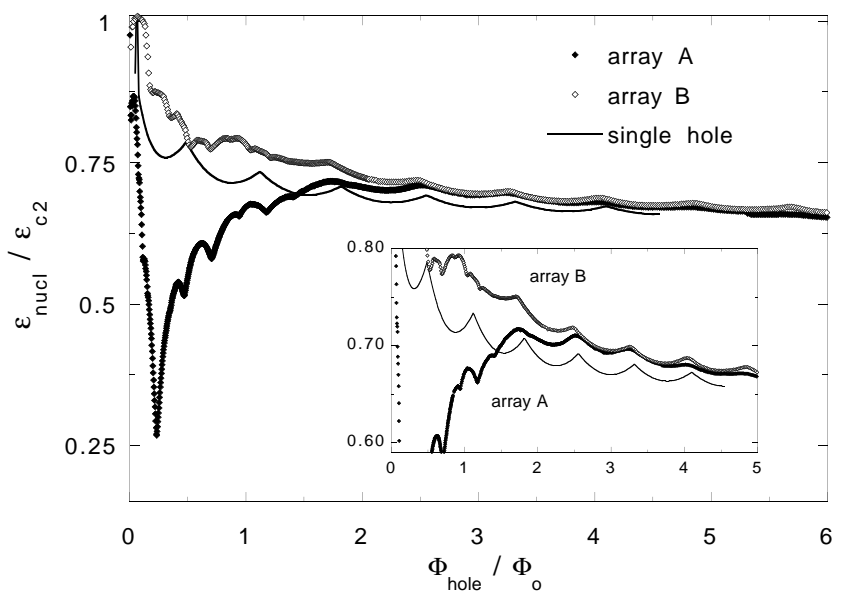


Fig. 2. Normalized nucleation energies $\epsilon_{nucl} / \epsilon_{c2}$ as a function of magnetic field (in units $HS_{hole}/\Phi_o = \Phi_{hole}/\Phi_o$), for sample A (solid dots), sample B (open diamonds) and the theoretical calculation for a cylindric cavity in an infinite thin film (solid line).

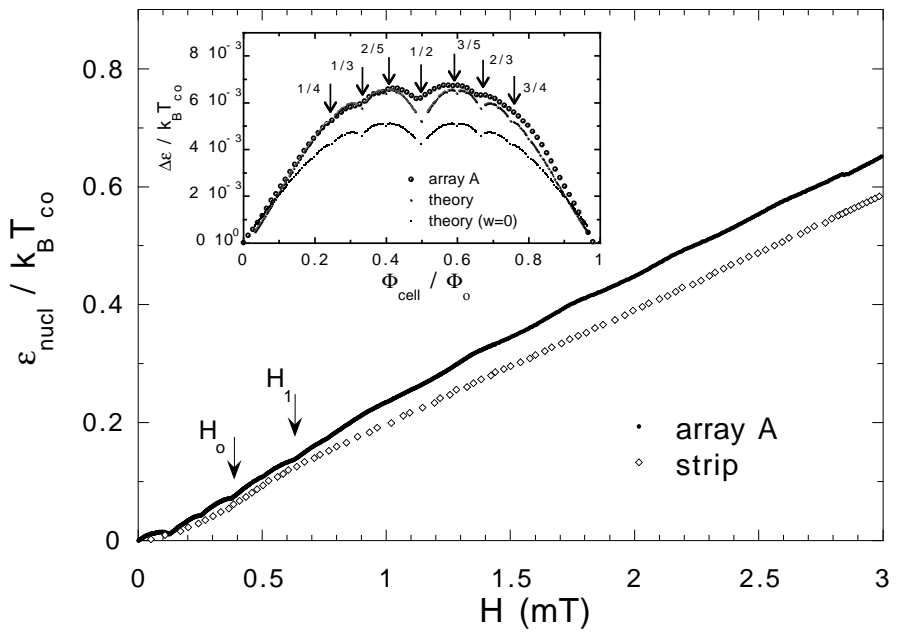


Fig. 3. Field dependence of the nucleation energies of array A (solid dots) and for a strip of width $w = 2.15\mu\text{m}$ (open diamonds), normalized by $k_B T_{\text{co}}$. In the field range $H_o < H < H_1$ interstitial vortices appear within strands. Inset: Coupling energy ϵ_{wnt} for array A (solid dots) and the theoretical ϵ_{wnt} for a superconducting wire network with $w = 0$ (small dots; lowest curve) and taking into account the wire thickness (small dots, upper curve) as a function of reduced field $\Phi_{\text{cell}} / \Phi_o$ between 0 and 1. The main dips position at rationals p/q are indicated by down arrows.

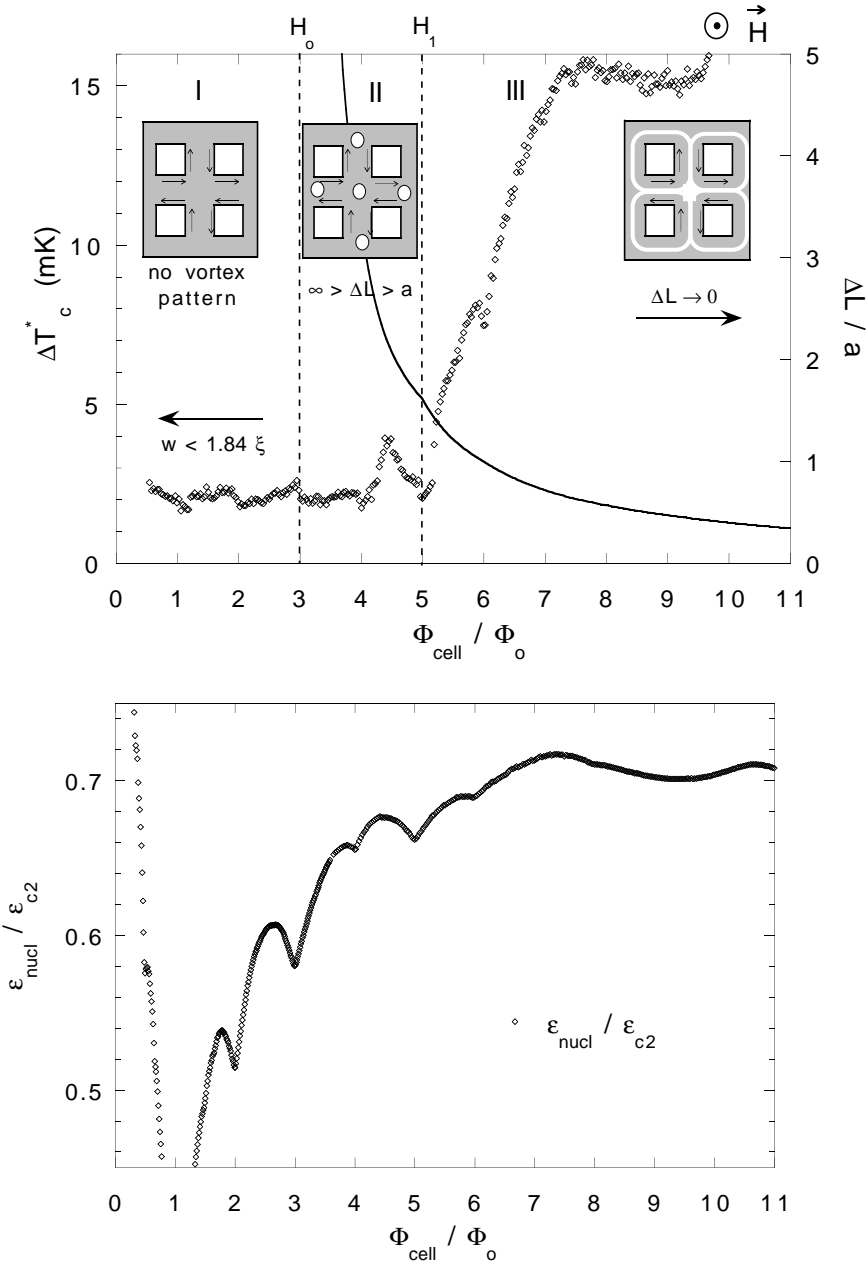


Fig. 4. a) Resistive transition width ΔT_c^* of array A (open diamonds) as a function of the reduced flux Φ_{cell}/Φ_o , and comparison with the normalized distance $\Delta L/a$ between interstitial vortices for a thin wire (solid line). An oversimplified picture of the vortex patterns developed within the wires is represented. Three main regions can be identified: (I) $w < 1.84\xi(T)$, nucleation starts symmetrically and there is no vortex in the wires; (II) $w > 1.84\xi(T)$ and $\infty > \Delta L/a \leq 1$, nodes of the order parameter appear at interstices due to the interference of neighbor edge wave functions (white dots); (III) $\Delta L/a < 1$ and decreases with increasing field until the surface solutions become independent and the single edge states are localized around each hole. b) field variation of the nucleation energy $\epsilon_{nucl}/\epsilon_{c2}$ for array A.

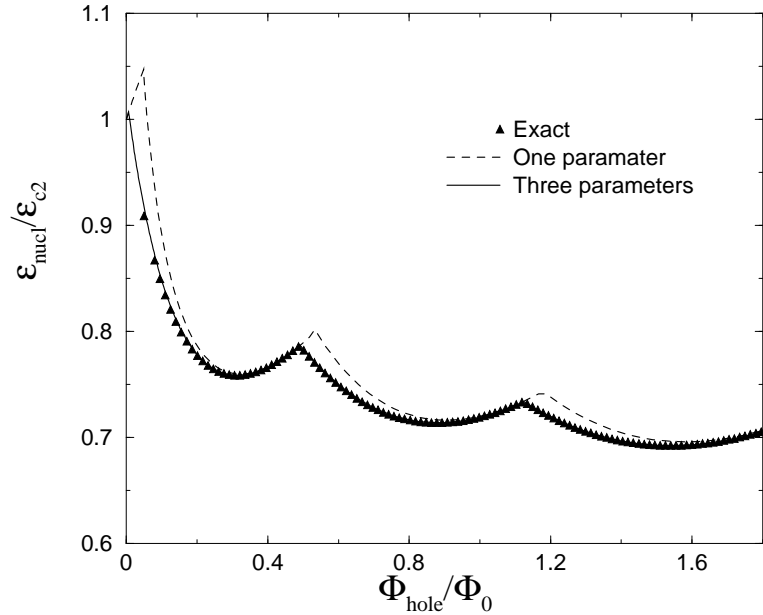


Fig. 5. Variational approximations for $\epsilon_{\text{nuc}}/\epsilon_{c2}$. The thick curve is obtained using the three parameter variational wave function. For comparison the curve obtained from the one parameter variational function is reported (dashed line).

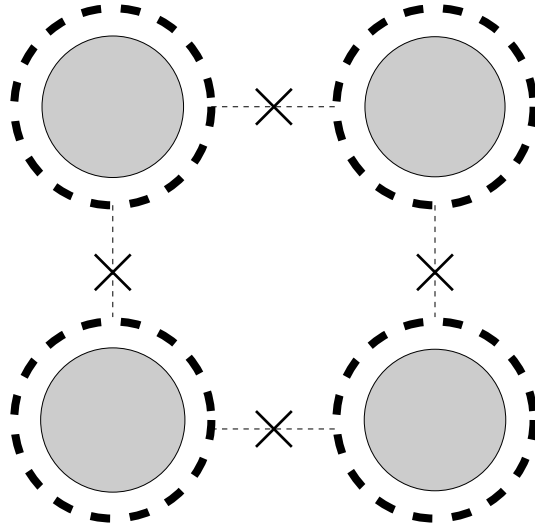


Fig. 6. Elementary cell of a square array of holes (grey circles). The edge states localized around each hole (thick dashed lines) are weakly coupled to first neighbor edge states. The coupling is indicated with crosses.

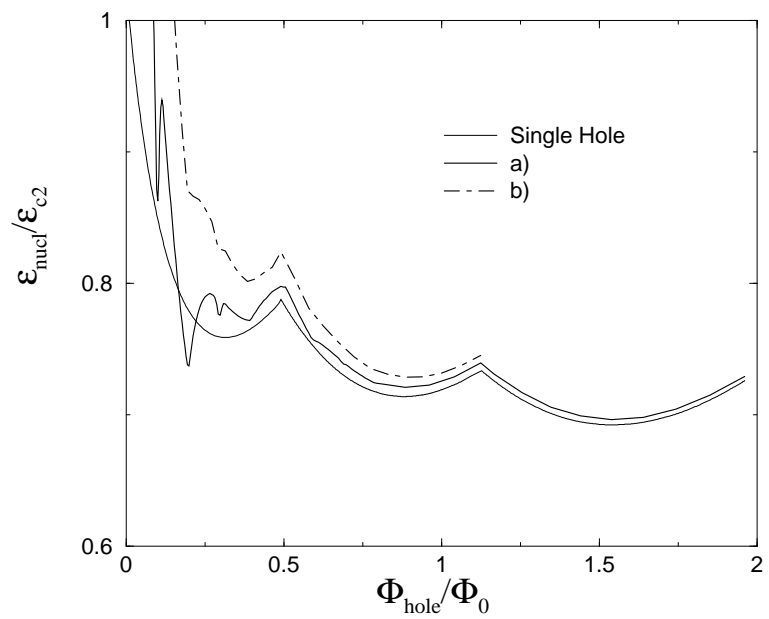


Fig. 7. The normalized nucleation energy $\epsilon_{nucl}/\epsilon_{c2}$ for a regular array of holes obtained by minimizing the functional as defined in the text for various parameter values: a) $g=0.1$ $g1=0.4$ $g2=1.6$; b) $g=0.2$ $g1=0.7$ $g2=0.9$.